RSC Advances

PAPER

View Article Online
View Journal | View Issue

Cite this: *RSC Adv.*, 2020, **10**, 8540

A Sm-MOF/GO nanocomposite membrane for efficient organic dye removal from wastewater†

Guohai Yang, ‡* Daqing Zhang,‡ Gen Zhu, Tingrong Zhou, Manting Song, Lulu Qu, Kecai Xiong * and Haitao Li*

The instability of graphene oxide (GO) membranes in aqueous solutions restricts their application in wastewater treatment through the membrane separation technology. In this work, a nanocomposite membrane (Sm-MOF/GO) composed of samarium metal–organic frameworks (Sm-MOFs) and GO nanosheets was successfully fabricated *via* the filtration of the corresponding Sm-MOF/GO dispersions. The *in situ* growth of Sm-MOF with aqueous stability on the GO sheets prevented the adjacent GO layers from expanding in aqueous solutions, thus endowing the prepared Sm-MOF/GO membrane with a stable membrane skeleton structure. Besides, the successful loading of Sm-MOF enlarged the layer space of the composite membrane, which was beneficial for higher permeance. The optimization of the Sm-MOF loading contents was also investigated to prepare M-*X* (where *X* represents the mass ratio of the MOF raw material to the total mass of the reactants). Subsequently, the fabricated M-0.31 possessed a high permeance of 26 L m^{-2} h^{-1} bar^{-1}, which was 3 times higher than that of a pure GO membrane; moreover, high rejections (>91%) to rhodamine B and methylene blue were obtained. After continuous 5.5 h filtration, the excellent rejection was still maintained as expected, indicating the long-term stability of M-0.31.

Received 5th February 2020
Accepted 12th February 2020

DOI: 10.1039/d0ra01110j

rsc.li/rsc-advances

1. Introduction

Organic dyes are widely used in various fields, such as textile, paint, leather and paper industries, and produce large quantities of wastewater containing dyes.[1,2] Most organic dyes are highly toxic, resistant to biodegradation and even carcinogenic;[3–5] thus, it is urgent to remove dyes from water. The conventional methods of the separation of pollutant dyes from water, such as distillation[6,7] crystallization and condensation, cannot achieve high separation efficiency. In recent decades, the membrane separation technology has been proven to be a promising approach to address the issue of environmental contaminants.[8–10] Compared to the traditional separation technology, membrane separation is more energy saving, easier to operate, and does not produce secondary pollution during the efficient separation of pollutant emissions; thus, it has great potential in the separation of water contaminants and water purification.[11–13]

As a two-dimensional nanomaterial researched widely in membrane separation, graphene oxide (GO) has been considered a strong competitor for liquid separation owing to its monoatomic thickness, lamellar structure, good membrane-forming ability, excellent mechanical strength and flexibility, and easy mass production characteristics.[14–16] However, there is no strong interaction between adjacent GO layers, thus leading to an expanded GO membrane when dispersed in an aqueous solution, which seriously affects the performance of the GO membrane. In this case, combining GO with other nanomaterials to build nanocomposites, purposefully adjusting the properties of the composites to reach the final separation target, becomes an effective approach to improve membrane performance.[17]

Thus, researchers focused on GO and metal–organic framework (MOF) nanocomposites.[18–21] As a network-like compound with the advantages of an adjustable structure, high porosity and large specific surface area,[22] MOF is constructed by combining a metal center and organic linkers *via* coordination bonds. The ultra-high specific surface area provides MOF with excellent adsorption properties for gas separation and storage, but weak dispersion forces attract small molecules, limiting the practical applications.[23] In addition, the instability of most MOFs dispersed in water solutions creates restrictions on water treatment. Interestingly, after the hybridization of GO and MOF, the forces between the GO layers are reinforced, and the dispersion of MOF in water is improved.[24] For example, Yang *et al.* prepared MOF@GO on cellulose acetate (CA) ultrafiltration membranes and found that the obtained CA/MOF@GO membranes exhibited higher hydrophilicity and pure water

School of Chemistry and Material Science, Jiangsu Normal University, Xuzhou 221116, China. E-mail: yangguohai@jsnu.edu.cn; kcxiong@jsnu.edu.cn; haitao@jsnu.edu.cn

† Electronic supplementary information (ESI) available. See DOI: 10.1039/d0ra01110j

‡ These authors contributed equally to this work.

flux.[25] Yang *et al.* fabricated a UiO-67/GO adsorbent and confirmed its enhanced adsorption capacity for an organophosphorus pesticide.[26] Although several MOF/GO nanocomposites have been explored, the research on MOF/GO membranes for water purification is very limited. Therefore, it is desirable to prepare diverse MOF/GO nanocomposites for applications in water purification.

In this work, a water-stable samarium MOF (Sm-MOF) was grown *in situ* on a GO layer to prepare a Sm-MOF/GO membrane through simple vacuum filtration. The optimization of the mass ratio (Sm-MOF to GO) was investigated, and the water flux and organic dye removal rates were immediately determined. As expected, the obtained Sm-MOF/GO membrane possessed larger interlayer space due to the *in situ* growth process. Moreover, the organic dye molecules were adsorbed by Sm-MOF with a three-dimensional network structure and then transferred to GO, which helped the fast and efficient removal of organic dyes from wastewater.

2. Experimental section

2.1. Materials

Concentrated sulfuric acid (H_2SO_4, 98%), 4,4′-bis(chloromethyl)-diphenyl, 1,3-benzene dicarboxylic acid (1,3-H_2bdc), samarium oxide (Sm_2O_3), phosphorus pentoxide (P_2O_5), potassium persulfate ($K_2S_2O_8$), potassium permanganate ($KMnO_4$), potassium nitrate (KNO_3), isonicotinic acid, hydrogen peroxide (H_2O_2, aq.), hydrochloric acid (HCl), rhodamine B (RhB), methylene blue (MB), bovine serum albumin (BSA), and dimethylformamide (DMF) were purchased from Aladdin (Shanghai, China). Graphite was purchased from BoYu material Company. Deionized water was produced by the Milli-Q reference system (18 MΩ cm^{-1}, Billerica, MA, USA). All chemicals were used directly without further purification.

2.2. Preparation of GO nanosheet suspensions

GO was fabricated through the modified Hummers' method.[27] Briefly, graphite powder (5 g) was added to a solution of H_2SO_4 (60 mL), $K_2S_2O_8$ (4.2 g) and P_2O_5 (4.2 g) at 80 °C and stirred for 4.5 h. After cooling naturally to room temperature followed by filtration, the solid expanded graphite was obtained; it was then was washed with a large amount of deionized water until it reached neutral pH. Then, the dried fluffy product (5 g) was added to concentrated H_2SO_4 (120 mL, 0 °C) and maintained at 10 °C. Afterwards, KNO_3 (2.5 g) and $KMnO_4$ (16 g) were added to the mixture and reacted at 35 °C for 2 h. Then, deionized water (250 mL) was added and continued for a further 2 h. Subsequently, deionized water (600 mL) and H_2O_2 (30 wt%, 30 mL) were added to the solution, and a gelatinous solid was obtained through standing overnight and filtration. Finally, the mixture was washed with HCl (1 M) solution and deionized water to remove metal ions and redundant acid, respectively; then, the GO powder was obtained after drying at 60 °C for 2 d. The GO suspension (2 mg mL^{-1}) used in this study was prepared *via* sonication of the GO powder in deionized water.

2.3. Preparation of the samarium-organic framework (Sm-MOF)

The samarium-organic framework (Sm-MOF) was prepared according to the method reported in literature.[28,29] The first step was the preparation of the ligand: 4,4′-bis(chloromethyl)-diphenyl (2.491 g) and isonicotinic acid (3.693 g) were dissolved in DMF (40 mL) and stirred for 8 h at 110 °C. After cooling down to room temperature, the precipitate was obtained by filtration. After washing with DMF and subsequent vacuum drying, white 1,4-bis(4-carboxylatopyridinium-1-methylene) benzene dichloride (H_2LCl_2) powder was obtained and it acted as a ligand. H_2LCl_2 (42 mg), 1,3-H_2bdc (32 mg), and Sm_2O_3 (35 mg) were added into a Teflon-lined stainless-steel container (20 mL), followed with deionized water (6 mL) addition and heating at 140 °C for 96 h. After cooling to room temperature, colorless crystals were obtained with further filtration and denoted as Sm-MOF.

2.4. The preparation of the Sm-MOF/GO nanocomposite

GO dispersion (12 mL), H_2LCl_2 (2.1 mg), 1,3-H_2bdc (1.6 mg), and Sm_2O_3 (1.7 mg) were added into a Teflon-lined stainless-steel container (20 mL) and then heated at 140 °C for 96 h. After cooling to room temperature, the reaction mixture was filtrated, followed by washing with deionized water. After drying at 60 °C, the Sm-MOF/GO nanocomposite was finally obtained. Sm-MOF/GO nanocomposite materials with different Sm-MOF loadings were prepared *via* an approach parallel to the above-mentioned approach with different amounts of GO. The prepared nanocomposite materials were named as M-*X*; *X* is the mass ratio of the MOF raw material with respect to the total mass of reactants. They were calculated as 0.18, 0.31, 0.41, 0.58 and 0.61.

2.5. Adsorption experiments

The adsorption performance of the materials was measured in RhB solutions (40 mL, 10 mg L^{-1}). Briefly, Sm-MOF/GO powders (10 mg) were added into the RhB solution under continuous stirring. Then, a small amount of the RhB solution was taken out at regular time intervals and was centrifuged to wipe Sm-MOF/GO powders out. Finally, the obtained RhB supernatant was detected by a UV-Vis spectrometer to acquire the concentration of the remaining RhB.

2.6. The preparation of Sm-MOF/GO nanocomposite membrane

The Sm-MOF/GO nanocomposite (15 mg) was dispersed in deionized water (30 mL) and sonicated for 12 h to obtain a suspension; then, the composite membrane was prepared on a PVDF polymer membrane through the vacuum filtration of the above suspension. On increasing the Sm-MOF loading, the prepared membranes were denoted as membrane-*X* (M-*X*), where *X* is the theoretical mass ratio of the MOF raw material in relation to the total mass of the reactants. The values were calculated as 0.18, 0.31, 0.41, 0.58 and 0.61, and the experimental values were 0.15, 0.20, 0.24, 0.36, and 0.59 (Table S1†).

2.7. Filtration experiments

The prepared M-*X* membranes were used to remove the organic dye RhB (30 mL, 10 mg L^{-1}) from water by vacuum filtration with a vacuum degree of 1 bar. The filtered liquor was collected and detected by UV-Vis spectroscopy. Subsequently, the rejection to RhB of the prepared M-*X* was calculated using the following formula: $\eta = (C_0 - C) \times C_0^{-1} = (A_0 - A) \times A_0^{-1} \times 100\%$; here, η is the rejection of the M-*X* membrane, C_0 and C are the concentrations of the RhB solutions before and after filtration, and A_0 and A are the ultraviolet curve absorbances of RhB before and after filtration, respectively. The permeance of M-*X* was calculated by the following formula: $J = V \times S^{-1} \times T^{-1} \times P^{-1}$; here, J is the permeance of M-*X*, V is the volume of RhB solution, S is the area of M-*X*, T is the filtration time, and P is the vacuum degree.

2.8. Characterization

The morphologies of the as-prepared nanocomposite membranes were characterized *via* a Scanning Electron Microscope (SEM, Hitachi SU8020, 10 kV) and Transmission Electron Microscope (TEM, JEOL JEM 1200EX, 120 kV). The thickness of the samples was measured *via* an Atomic Force Microscope (AFM). The crystal structure of the samples was investigated by X-Ray Diffraction (XRD) using a Bruker D8 advance diffractometer with Cu-Kα source. The bonding of the samples was obtained through Fourier Transform Infrared Spectroscopy (FTIR, Thermo Electron Antaris II). The concentration of the organic dyes was measured using UV-Vis spectroscopy (Thermo Fisher Scientific, NanoDrop 2000c). The actual content of Sm-MOF on GO was measured by Inductively Coupled Plasma (ICP, Agilent ICPOES730). The water contact angles of the Sm-MOF/GO composite membrane were measured through an interfacial tension-meter (DCAT21).

3. Results and discussion

3.1. Characterization and mechanism

The mechanism of dye removal from water through the Sm-MOF/GO composite membrane is shown in Fig. 1. Sm-MOF, with good stability in water, was grown *in situ* on the GO layer, which connected the adjacent GO layers and thus prevented the GO membrane expansion in aqueous solutions. Meanwhile, the layer spacing of the GO membrane increased

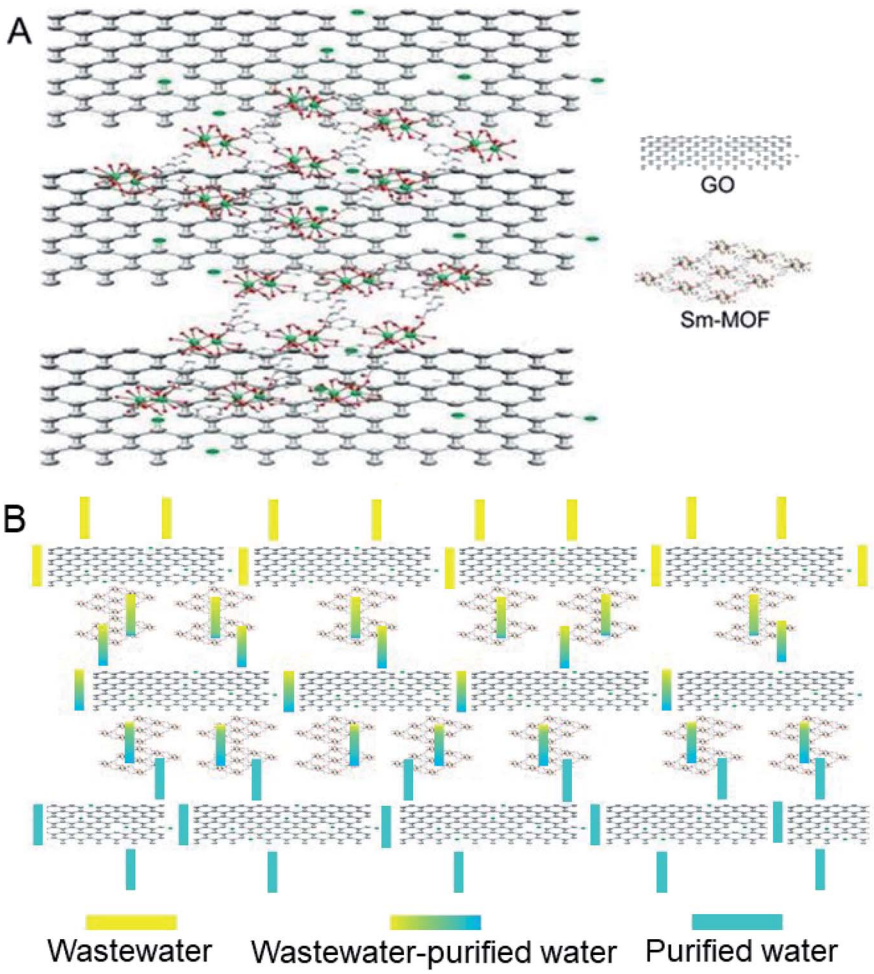

Fig. 1 Schematic illustration of (A) Sm-MOF/GO nanocomposite membranes. (B) A possible route for dye removal from water through the membrane.

due to the introduction of Sm-MOF, which improved membrane permeance. Moreover, Sm-MOF exhibited a three-dimensional network structure, which facilitated the interception of pollutant molecules when the pollutants were transported into the GO sheets, thereby achieving better separation performance.

SEM and TEM were performed to observe the structure and morphology of the prepared materials; the results are shown in Fig. 2. It can be seen that the prepared GO nanosheets are papery with a lateral dimension of 500–1000 nm (Fig. 2A and B). Sm-MOF is shaped like a slender bar, as observed from the SEM and TEM images (Fig. 2C and D), and it can grow further to obtain a block crystal. After the *in situ* growth of Sm-MOF on the GO sheets, the Sm-MOF/GO nanocomposite was obtained, and it could be seen that Sm-MOF was successfully loaded onto the GO sheets (Fig. 2E and F). The obtained GO and Sm-MOF/GO membrane morphologies are shown in Fig. 2G and H, respectively. Compared to the GO membrane, the Sm-MOF/GO membrane performed strongly due to its network structure mentioned above. It should be mentioned that the membrane was flexible and stable in water.

XRD patterns of the prepared GO, Sm-MOF, and Sm-MOF/GO nanocomposites were recorded, as shown in Fig. 3A and B. The diffraction peaks of GO and Sm-MOF were the same as

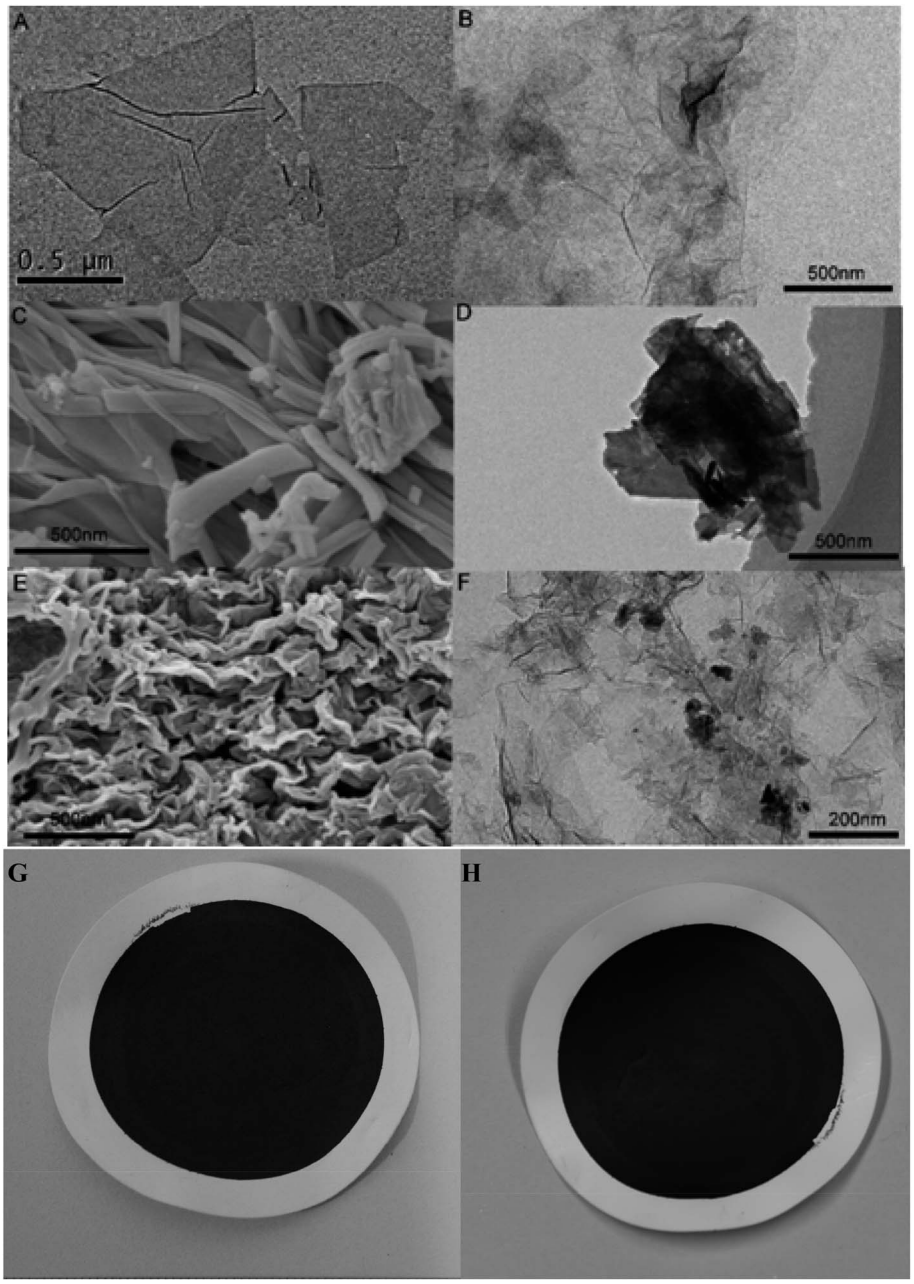

Fig. 2 (A) SEM and (B) TEM images of GO; (C) SEM and (D) TEM images of Sm-MOF; (E) SEM and (F) TEM images of Sm-MOF/GO nanocomposite membrane; optical images of (G) GO and (H) Sm-MOF/GO membranes.

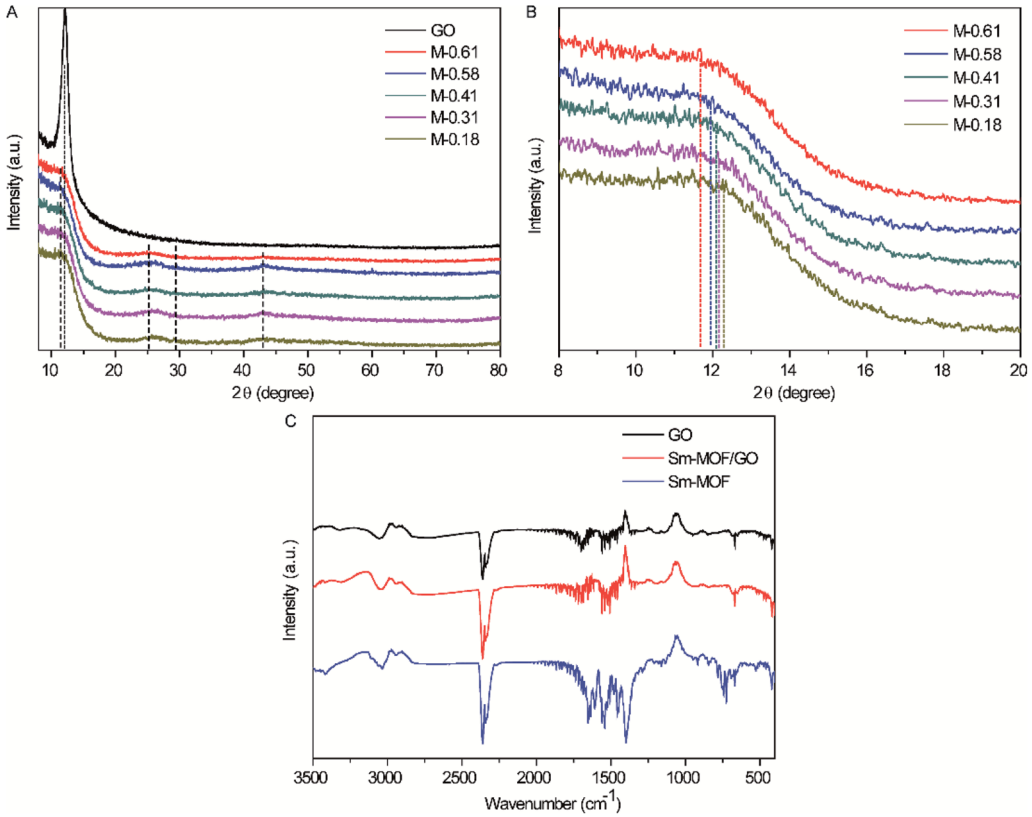

Fig. 3 (A) XRD pattern, (B) amplified XRD view, and (C) FTIR spectra of prepared GO, Sm-MOF, and Sm-MOF/GO.

those reported in literature[28,30] and appeared in the XRD patterns of the Sm-MOF/GO composites. As shown in Fig. 3A, the diffraction peak of the pristine GO membrane is located at 12.2°, and it shifts to the left on embedding Sm-MOF, which indicates the enlarged GO layer space. Besides, with the increase in the Sm-MOF loading capacity, more left-shifted peaks are observed (Fig. 3B), which means that a more Sm-MOF loading content contributes to the more enlarged GO layer space. In order to confirm the successful growth of Sm-MOF on the GO nanosheets, the binding interactions of the prepared materials were measured through FTIR spectroscopy (Fig. 2B). The absorption peaks for GO are seen at 3403 cm^{-1}, 1729 cm^{-1}, and 1620 cm^{-1}, which correspond to the O–H, C=O, and C=C stretching vibrations, indicating that thin GO nanosheets have been successfully synthesized with graphite as a precursor. In addition, the diffraction peaks of the Sm-MOF/GO composites overlap with that of GO and Sm-MOF, further confirming the successful synthesis of the Sm-MOF/GO composites.

The performance of the prepared GO and Sm-MOF/GO for the adsorption of RhB was measured, as shown in Fig. 4. Although the adsorption rate of Sm-MOF/GO was significantly inferior to that of GO, similar saturated adsorption amounts were obtained and were calculated to be 32 and 36 mg g^{-1}, respectively, indicating that certain adsorption abilities of the prepared GO and Sm-MOF/GO materials were achieved.

The cross-sectional images of the prepared composite membranes are shown in Fig. 5. GO and Sm-MOF are clearly observed on M-0.31 with a thickness of 2.2 μm (Fig. 5A). The membrane skeleton was constructed through the stacking of GO sheets, and the interlayer space of the GO membrane increased after the Sm-MOF loading, which contributed to an increase in the Sm-MOF/GO membrane permeance (Fig. 5B). On increasing the mass of Sm-MOF, the GO layer stacking was inhibited with the gradual growth of the Sm-MOF crystals, which prevented the construction of the membrane skeleton (Fig. 5C and D). This may lead to a sharp decrease in the dye

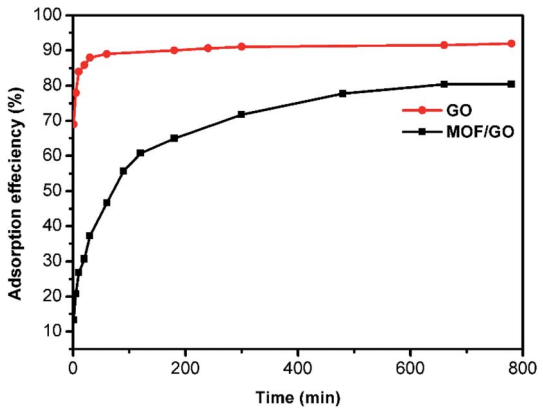

Fig. 4 The static adsorption of GO and Sm-MOF/GO nanocomposite to RhB.

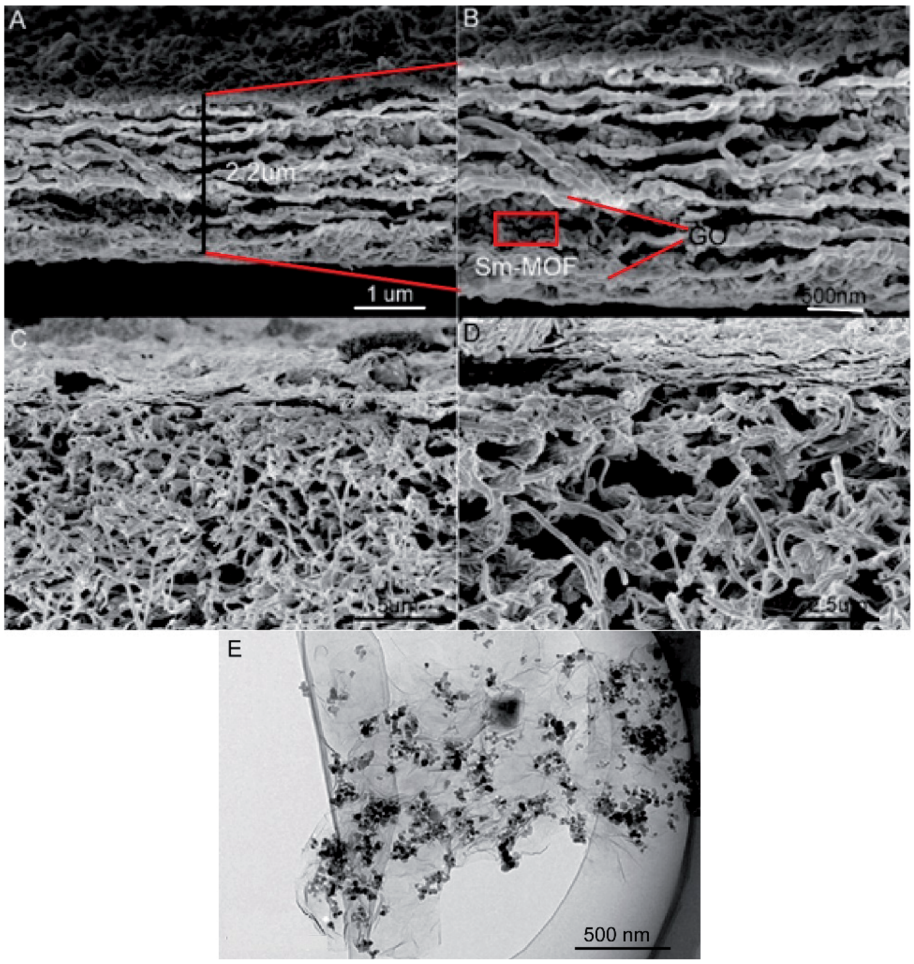

Fig. 5 (A and B) Cross-section images of the prepared M-0.31; (C and D) cross-section images of the prepared M-0.41; (E) TEM image of M-0.31.

rejection rate in the presence of M-0.41. The uniform growth of Sm-MOF between the GO layers can be clearly seen from the TEM image of M-0.31 (Fig. 5E), which is consistent with the SEM result (Fig. 5A and B).

3.2. Membrane performances

The filtration performances of the prepared GO and M-*X* membranes were investigated by filtering RhB solutions (10 mg mL^{-1}, 30 mL). As shown in Fig. 6A, the maximum absorbance of RhB at 554 nm decreases when filtered by the GO membrane and different M-*X* membranes, indicating the successful removal of RhB molecules in solution. Besides, with the increased mass contents of Sm-MOF in the nanocomposite membranes, the maximum absorbance of RhB at 554 nm increased gradually, demonstrating reduced removal efficiency. Therefore, it is necessary to explore M-*X* possessing excellent

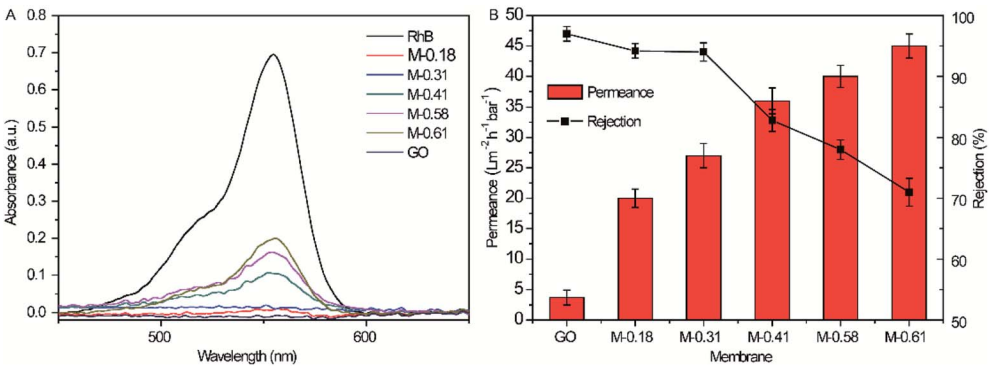

Fig. 6 (A) UV-Vis absorption of initial RhB solution and the filtrate filtrated by GO membrane and M-*X*; (B) filtration performance of GO membrane and M-*X*.

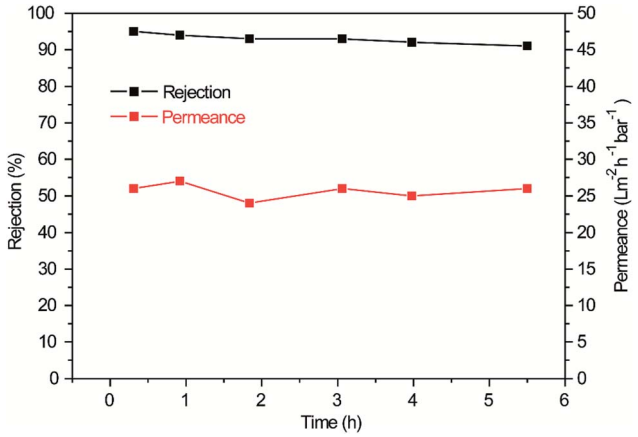

Fig. 7 The rejection effectiveness and water permeance *versus* time of M-0.31.

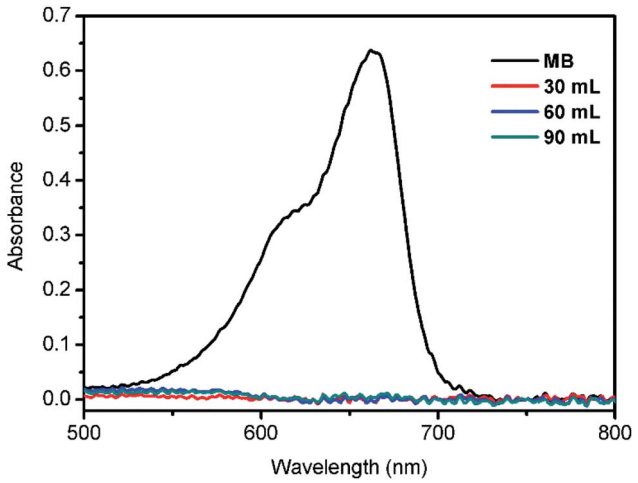

Fig. 8 UV-Vis absorption of initial MB solution and filtrate filtrated by the M-0.31.

permeance and rejection, as concluded in Fig. 6B. On increasing the Sm-MOF loading, the permeance of the prepared composite membrane increased mainly due to the increased interlayer spacing caused by increasing Sm-MOF. The water contact angles decreased by increasing the Sm-MOF loading, it may be another reason for the increased permeance of the prepared composite membrane (Fig. S1†).[31] The rejection to the dyes decreased gradually with the increase in MOF due to the irregular membrane skeleton caused by the inhibited stacking of the GO layers. Besides, the comparable pure water permeance recovery rate (65.54%) indicated that the prepared M-0.31 possessed a certain antifouling property for BSA (Table S2†). Therefore, the composite membrane M-0.31, possessing the highest permeance and rejection and comparable antifouling property, is an excellent candidate for further applications in wastewater treatment.

Fig. 7 shows the rejection effectiveness and water permeance *versus* time of M-0.31. The M-0.31 rejection to RhB was as high as 95%, and this result was comparable to previous reports.[18,32,33] In addition, the permeance of M-0.31 was stable at 26 L m^{-2} h^{-1} bar^{-1}, which was 3 times higher than that of the pure GO membrane and also comparable to other works.[34,35] After 5.5 h filtration, the rejection was highly contained without a significant decrease in some time, indicating the good stability of M-0.31. The water permeance and rejection were significantly reduced in 100 h. The reduced water permeance may be attributed mainly to the aggregation of more RhB molecules on the membrane surface and between the interlayers of the GO sheets, leading to crowded channels and a longer time for water circulation. The reduced rejection may be mainly attributed to the affected membrane skeleton due to the longer time of immersion in the water solution.

The performance of M-0.31 for the removal of MB (5 mg L^{-1}, 90 mL) from water was also analyzed; the UV-visible absorption spectrum of the MB filtrate is shown in Fig. 8. It can be clearly seen that the maximum absorbance of the MB filtrate is reduced drastically, indicating the effective MB removal from water through the as-prepared M-0.31. Overall, it can be concluded that the prepared composite M-0.31 may be a potential candidate for efficient wastewater treatment.

4. Conclusion

In short, Sm-MOF/GO dispersions were prepared by the *in situ* growth of Sm-MOF on the GO nanosheets, followed by the fabrication of a series of Sm-MOF/GO nanocomposite membranes, *i.e.*, M-*X via* facile vacuum filtration of the corresponding Sm-MOF/GO dispersions. The optimization of the Sm-MOF loading contents was investigated and the M-0.31 composite possessed stable permeance (26 L m^{-2} h^{-1} bar^{-1}) and rejection (>91%) to the organic dye RhB due to the combination of the Sm-MOF framework structure and the GO lamellar structure. After continuous 5.5 h filtration, the rejection was highly contained without a significant decrease, indicating the long-term stability of M-0.31. Therefore, the fabricated M-0.31 may be a potential candidate for actual wastewater treatment.

Conflicts of interest

There are no conflicts to declare.

Acknowledgements

This work was financially supported by the National Natural Science Foundation of China (21605062, 21974055).

References

1 P. Sathishkumar, R. Sweena, J. J. Wu and S. Anandan, *Chem. Eng. J.*, 2011, **171**, 136–140.
2 R. Y. Hong, J. H. Li, L. L. Chen, D. Q. Liu, H. Z. Li, Y. Zheng and J. Ding, *Powder Technol.*, 2009, **189**, 426–432.
3 Z. Cai, Y. Sun, W. Liu, F. Pan, P. Sun and J. Fu, *Environ. Sci. Pollut. Res.*, 2017, **24**, 15882–15904.

4 E. Akceylan, M. Bahadir and M. Yılmaz, *J. Hazard. Mater.*, 2009, **162**, 960–966.
5 S. Dai, W. Song, Y. Zhuang and H. Yan, Biotechnical treatment of wastewater containing Azo dyes, in *Proceedings of the 4th Mainland–Taiwan Environmental Technology Seminar*, 1996, vol. 1, pp. 407–411.
6 E. Curcio and E. Drioli, *Sep. Purif. Rev.*, 2005, **34**, 35–86.
7 A. Fahmy, D. Mewes and K. Ebert, *Sep. Sci. Technol.*, 2001, **36**, 3287–3304.
8 S. Kim, H. Wang and Y. M. Lee, *Angew. Chem., Int. Ed.*, 2019, **58**, 17512–17517.
9 G. Liu, W. Jin and N. Xu, *Angew. Chem., Int. Ed.*, 2016, **55**, 13384–13397.
10 L. Qu, G. Zhu, J. Ji, T. Yadav, Y. Chen, G. Yang, H. Xu and H. Li, *ACS Appl. Mater. Interfaces*, 2018, **10**, 42427–42435.
11 A. Khalid, M. Aslam, M. A. Qyyum, A. Faisal, A. L. Khan, F. Ahmed, M. Lee, J. Kim, N. Jang, I. S. Chang, A. A. Bazmi and M. Yasin, *Renewable Sustainable Energy Rev.*, 2019, **105**, 427–443.
12 D. Qian, D. Chen, N. Li, Q. Xu, H. Li, J. He and J. Lu, *J. Membr. Sci.*, 2018, **554**, 16–25.
13 R. Zhang, Y. Liu, M. He, Y. Su, X. Zhao, M. Elimelech and Z. Jiang, *Chem. Soc. Rev.*, 2016, **45**, 5888–5924.
14 T. Yang, H. Lin, K. P. Loh and B. Jia, *Chem. Mater.*, 2019, **31**, 1829–1846.
15 Y.-C. Du, L.-J. Huang, Y.-X. Wang, K. Yang, J.-G. Tang, Y. Wang, M.-M. Cheng, Y. Zhang, M. J. Kipper, L. A. Belfiore and W. S. Ranil, *J. Appl. Polym. Sci.*, 2019, **136**, 47761.
16 W.-S. Hung, Y.-H. Chiao, A. Sengupta, Y.-W. Lin, S. R. Wickramasinghe, C.-C. Hu, H.-A. Tsai, K.-R. Lee and J.-Y. Lai, *Carbon*, 2019, **142**, 337–345.
17 X. Wang, M. Feng, Y. Liu, H. Deng and J. Lu, *J. Membr. Sci.*, 2019, **577**, 41–50.
18 J. Ma, X. Guo, Y. Ying, D. Liu and C. Zhong, *Chem. Eng. J.*, 2017, **313**, 890–898.
19 Y. Ying, D. Liu, W. Zhang, J. Ma, H. Huang, Q. Yang and C. Zhong, *ACS Appl. Mater. Interfaces*, 2017, **9**, 1710–1718.
20 S. Castarlenas, C. Téllez and J. Coronas, *J. Membr. Sci.*, 2017, **526**, 205–211.
21 S. Yang, Q. Zou, T. Wang and L. Zhang, *J. Membr. Sci.*, 2019, **569**, 48–59.
22 Y. Liu, Y. Ban and W. Yang, *Adv. Mater.*, 2017, **29**, 1606949.
23 Z. Kang, L. Fan and D. Sun, *J. Mater. Chem. A*, 2017, **5**, 10073–10091.
24 M. D. Firouzjaei, A. A. Shamsabadi, S. A. Aktij, S. F. Seyedfour, M. Sharifian Gh, A. Rahimpour, M. R. Esfahani, M. Ulbricht and M. Soroush, *ACS Appl. Mater. Interfaces*, 2018, **10**, 42967–42978.
25 S. Yang, Q. Zou, T. Wang and L. Zhang, *J. Membr. Sci.*, 2019, **569**, 48–59.
26 Q. Yang, J. Wang, W. Zhang, F. Liu, X. Yue, Y. Liu, M. Yang, Z. Li and J. Wang, *Chem. Eng. J.*, 2017, **313**, 19–26.
27 L.-L. Qu, N. Wang, Y.-Y. Li, D.-D. Bao, G.-H. Yang and H.-T. Li, *J. Mater. Sci.*, 2017, **52**, 8311–8320.
28 Y.-L. Gai, Q. Guo, X.-Y. Zhao, Y. Chen, S. Liu, Y. Zhang, C.-X. Zhuo, C. Yao and K.-C. Xiong, *Dalton Trans.*, 2018, **47**, 12051–12055.
29 J.-K. Sun, P. Wang, C. Chen, X.-J. Zhou, L.-M. Wu, Y.-F. Zhang and J. Zhang, *Dalton Trans.*, 2012, **41**, 13441–13446.
30 R. Castro-Munoz, J. Buera-Gonzalez, O. de la Iglesia, F. Galiano, V. Fila, M. Malankowska, C. Rubio, A. Figoli, C. Tellez and J. Coronas, *J. Membr. Sci.*, 2019, **582**, 423–434.
31 Y. Q. Zhang, X. B. Yang, Z. X. Wang, J. Long and L. Shao, *J. Mater. Chem. A*, 2017, **5**, 7316–7325.
32 H. Fan, J. Gu, H. Meng, A. Knebel and J. Caro, *Angew. Chem., Int. Ed.*, 2018, **57**, 4083–4087.
33 Z. Rao, K. Feng, B. Tang and P. Wu, *ACS Appl. Mater. Interfaces*, 2017, **9**, 2594–2605.
34 J. Wang, Y. Wang, Y. Zhang, A. Uliana, J. Zhu, J. Liu and B. Van der Bruggen, *ACS Appl. Mater. Interfaces*, 2016, **8**, 25508–25519.
35 W. L. Xu, C. Fang, F. Zhou, Z. Song, Q. Liu, R. Qiao and M. Yu, *Nano Lett.*, 2017, **17**, 2928–2933.